Effect of Sulfur Oxyanions and Magnetite Deposits on the Corrosion Behavior of Alloy 600 in Simulated Crevice Environments

Do Haeng Hur [a*], Jeoh Han [b], Soon-Hyeok Jeon [a], Geun Dong Song [c]
[a] *Nuclear Materials Safety Research Division, Korea Atomic Energy Research Institute, Daejeon 34057*
[b] *Central Research Institute of Korea Hydro & Nuclear Power Co., Ltd, Daejeon 34101*
[c] *Nuclear Materials Research Group, FNC Technology Co. Ltd, Yongin 17084*
[*] *Corresponding author: dhhur@kaeri.re.kr*

Keywords : Alloy 600, magnetite deposit, sulfate, tetrathionate, galvanic corrosion

1. Introduction

Sulfate ions (SO_4^{2-}) in the secondary water of PWRs originate from seawater leakage and cation resin beads. Although the initial ingress is in the form of sulfate ions, sulfur can exist in various valence states such as −2 (sulfide, S^{2-}), +2 (thiosulfate, $S_2O_3^{2-}$), +2.5 (tetrathionate, $S_4O_6^{2-}$), +4 (sulfite, SO_3^{2-}), and +6 (sulfate, SO_4^{2-}) in the secondary water conditions [1]. These reduced sulfur species can cause intergranular attack, pitting, and stress corrosion cracking of Ni-based alloys [2-4].

Meanwhile, magnetite behaves like a metal due to its high electrical conductivity. As a result, when a metal and magnetite deposits are electrically contacted, galvanic coupling effect increases the corrosion current density of Ni-based alloys and carbon steels in various solutions [5-9]. To date, most studies on the corrosion behavior of Ni-based alloys have been conducted in solutions containing only a single type of sulfur species, either sulfate ions or reduced sulfur independently [4,10,11]. Therefore, the objective of this study was to investigate the corrosion behavior of Alloy 600 coupled with magnetite in simulated PWR secondary water containing sulfur oxyanions (sulfate and tetrathionate). This test condition was designed to simulate the corrosion phenomenon taking place in water-filled pores within porous magnetite deposits deposited on Alloy 600 steam generator (SG) tubes.

2. Experimental Methods

2.1 Preparation of U-bend Specimens

Alloy 600 specimens with the dimensions of 7 × 24.4 × 1.25 mm were ground with SiC paper and then ultrasonically cleaned in acetone for 10 min. They were bent into a U-bend shape in accordance with ASTM G30-97. After bending, the straight region of the specimen was fastened to apply constant stress using an Alloy 600 bolt and nut.

Magnetite-deposited specimens were manufactured by electrodepositing a magnetite layer over the entire surfaces of the U-bend specimens except for a width of approximately 500 μm along the apex as shown in Fig. 1. Here, the magnetite-free apex region corresponds to the local environment of pores within the porous magnetite deposits on the surfaces of actual SG tubes. Accordingly, a galvanic coupling between Alloy 600 and magnetite was expected to be formed in the exposed apex region. The solution used for electrodeposition consisted of 2 M NaOH, 0.1 M triethanolamine and 0.043 M $Fe_2(SO_4)_3$.

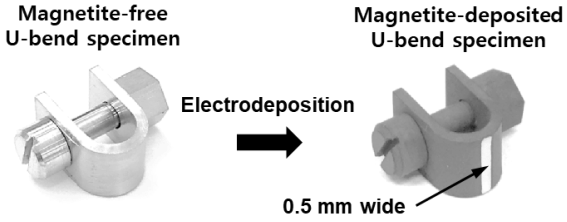

Fig. 1. Preparation of magnetite-deposited U-bend specimens.

2.2 Immersion Corrosion Tests

Immersion corrosion tests were conducted under three different conditions at 340 °C for 500 h, as presented in Table 1. Reference solution was prepared by adding ethanolamine to deionized water until the pH reached pH 9.0±0.1 at 25 °C. The mixed sulfur oxyanions solution was prepared by adding sulfur oxyanions (0.05 M Na_2SO_4 + 0.01 M $Na_2S_4O_6$) into the reference solution.

Table 1. Test conditions

	Test solution	Specimen type	Others
1	Reference solution (sulfur oxyanions-free)	Magnetite-free U-bend	340°C 500 h
2	Mixed sulfur oxyanions solution (reference solution + 0.05 M Na_2SO_4 + 0.01 M $Na_2S_4O_6$)	Magnetite-free U-bend	
3		Magnetite-deposited U-bend	

2.3 Electrochemical Corrosion Tests

The electrochemical corrosion behavior of Alloy 600, pure Ni, pure Cr, and magnetite were investigated in each test solution shown in Table 1 at 80 °C. Notably, a magnetite working electrode was made by

electrodepositing a magnetite layer onto the entire surface of the Alloy 600 working electrode.

3. Results and Discussion

Fig. 2 shows cross-sectional images formed on the apex region of the U-bend specimens after the immersion corrosion tests in each test condition. No localized corrosion such as stress corrosion crack, intergranular attack and pitting, was observed in all test conditions. The magnetite-free U-bend specimens in the reference solution appeared, as if no corrosion had occurred at all, and the oxide layer was too thin to be identified. On the other hand, a very thick oxide layer was observed in the mixed sulfur oxyanions solution. A thick oxide layer of approximately 180 μm was formed on the magnetite-free U-bend specimens, while an even thicker oxide layer of approximately 300 μm was formed on the magnetite-deposited U-bend specimens. This indicates that sulfur oxyanions accelerate the corrosion rate of Alloy 600. Furthermore, when sulfur oxyanions interact with magnetite, corrosion rate further accelerates due to their combined effect.

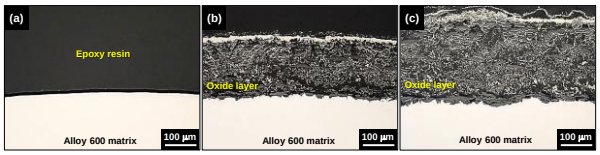

Fig. 2. Cross-sectional images of the U-bend specimens after the immersion corrosion tests at 340 ℃ for 500 h: (a) magnetite-free U-bend specimen in the reference solution, (b) magnetite-free U-bend specimen in the mixed sulfur oxyanions solution, and (c) magnetite-deposited U-bend specimen in the mixed sulfur oxyanions solution.

Fig. 3 and Table 2 show the cross-sectional SEM images and chemical compositions of the oxide layers formed in the mixed sulfur oxyanions solutions, respectively. The morphology and chemical compositions of the oxide layers were almost the same for both the magnetite-free and magnetite-deposited U-bend specimens.

At the bottom section, the oxide layer (point 1) adjacent to the alloy matrix was significantly depleted in Ni and enriched in Cr and Fe compared to the matrix. Small particles (point 2) were identified as Ni_3S_2 compounds. Because point 3 was composed of carbon and oxygen, it is believed that the epoxy resin used to mount the specimen permeated the vacant spaces of the loose oxide. The middle section of the oxide contained Ni-depleted Cr-Fe oxides with a longish shape (point 4) and Ni_3S_2 compounds (point 5). Since the chemical compositions of points 1 and 4 were similar to each other, it is apparent that the Ni-depleted Cr-Fe oxides of point 1 were separated from the Alloy 600 matrix. The oxide layer closer to the test solution was composed of Ni-depleted Cr-Fe oxides with a longish shape (point 6) and Ni_3S_2 compounds with a clustered line-shape (point 7), respectively.

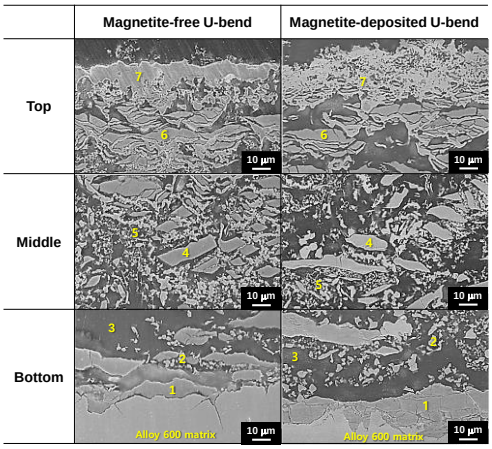

Fig. 3. SEM images of the cross-sections of the U-bend specimens in the mixed sulfur oxyanions solution. The numbers on the images indicate the locations where the EDS point analyses were performed (See Table 2).

Table 2. Chemical compositions of the oxide layers formed on the U-bend specimens in the mixed sulfur oxyanions solution using EDS point analyses (at.%).

Magnetite-free U-bend specimen						
Point	Ni	Cr	Fe	S	O	C
1	8.6	18.7	11.3	2.2	59.2	
2	57.6	0.4	0.8	34.3	6.9	-
3	-	-	-	-	12.4	87.6
4	7.6	19.6	11.5	0.5	60.8	
5	60.2	0.5	0.1	34.9	4.3	
6	6.2	21.4	11.6	0.5	60.3	
7	55.9	0.26	0.27	38.8	4.77	-

Fig. 4 shows the polarization curves of Alloy 600 in the reference, sulfate, and mixed sulfur oxyanions solution at 80 °C. The polarization behavior of Alloy 600 was quite similar in both the reference and sulfate solutions. On the other hand, the corrosion potential (E_{corr}) of Alloy 600 was approximately 110 mV higher in the mixed sulfur oxyanions solution than in the reference solution. The passivity was breakdown around −0.35 V_{SCE} and then the anodic current density was actively increased in the mixed sulfur oxyanions solution. These results indicate that tetrathionate, not sulfate, primarily increases corrosion potential and current density by acting as an oxidizer.

As shown in Fig. 5, the E_{corr} of Alloy 600 was about 310 mV lower than that of magnetite. Therefore, when Alloy 600 is electrically connected to magnetite like the magnetite-deposited U-bend specimens, Alloy 600 will behave as an anode, while the magnetite will behave as a cathode. In addition, when the area ratio of magnetite to Alloy 600 increases from 1 to 45, the galvanic current density of Alloy 600 will significantly increase.

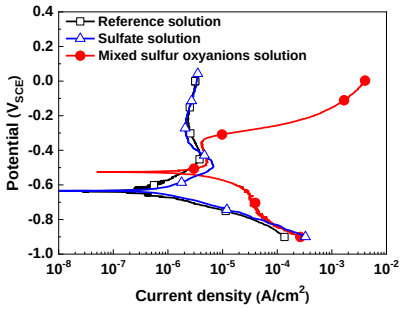

Fig. 4. Potentiodynamic polarization curves of Alloy 600 in each test solution at 80 °C.

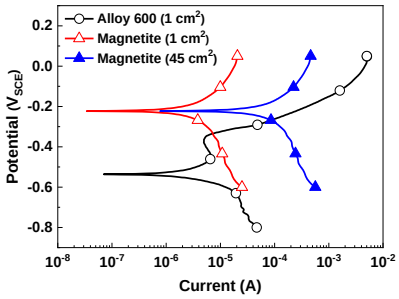

Fig. 5. Potentiodynamic polarization curves of Alloy 600 and magnetite in the mixed sulfur oxyanions solution at 80 °C.

Fig. 6 shows the polarization behavior of pure Cr and pure Ni in the reference and mixed sulfur oxyanions solutions. Both the anodic and cathodic current density of Cr were barely affected by sulfur oxyanions, although the E_{corr} was about 160 mV higher in the mixed sulfur oxyanions solution. Passivation behavior was clearly observed in both solutions. In contrast, Ni did not exhibit a stable passive state even in the reference solution, although weak active-passive transition behavior was observed. In addition, Ni was actively dissolved without passivation and the i_{corr} of Ni was much more than 2-orders of magnitude greater in the mixed sulfur oxyanions solution than in the reference solution. Therefore, the passivity breakdown of Alloy 600 at −0.35 V_{SCE} in the mixed sulfur oxyanions solution (Fig. 4) is attributed to the active dissolution of Ni. Based on the polarization curves, it appears that corrosion of Alloy 600 is primarily governed by the selective dissolution of Ni. This electrochemical behavior is consistent with the formation of the Ni-depleted oxides in the mixed sulfur oxyanions solution.

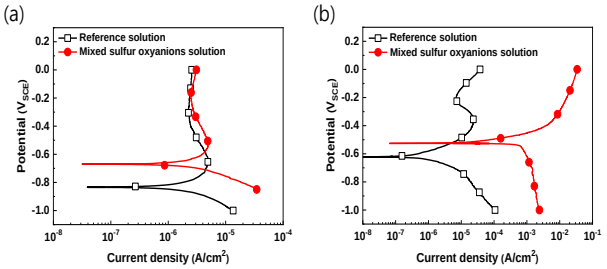

Fig. 6. Potentiodynamic polarization curves in each test solution at 80 °C: (a) pure Cr, (b) pure Ni.

4. Conclusions

1) The electrochemical corrosion current and oxide thickness of Alloy 600 are drastically increased in the presence of mixed sulfur oxyanions. These results are attributed to the preferential dissolution of alloying element Ni. Based on the polarization curves, this change is primarily caused by tetrathionate, not sulfate.

2) When Alloy 600 is coupled with magnetite in the mixed sulfur oxyanions solution, the alloy and magnetite behave as an anode and cathode, respectively. This galvanic couple results in the increase in the corrosion current density and oxide thickness of Alloy 600.

Acknowledgements

This study was funded by the National Research Foundation of the Republic of Korea (RS-2022-00143316).

REFERENCES

[1] Z. Fang, R.W. Staehle, Effects of the valence of sulfur on passivation of Alloys 600, 690, and 800 at 25 °C and 95 °C, Corrosion 55 (1999) 355–379.
[2] R.W. Staehle, J.A. Gorman, Quantitative assessment of submodes of stress corrosion cracking on the secondary side of steam generator tubing in pressurized water reactors, Corrosion 59 (2003) 931–994.
[3] K. Frizzetti, Pressurized water reactor secondary water chemistry guidelines – Revision 7, EPRI, 2009.
[4] I.J. Yang, Effect of sulphate and chloride ions on the crevice chemistry and stress corrosion 395 cracking of Alloy 600 in high temperature aqueous solutions, Corros. Sci. 33 (1992) 25–37.
[5] S.H. Jeon, G.D. Song, D.H. Hur, Corrosion behavior of Alloy 600 coupled with electrodeposited magnetite in simulated secondary water of PWRs, Mater. Trans. 56 (2015) 2078–2083.
[6] G.D. Song, S.H. Jeon, J.G. Kim, D.H. Hur, Synergistic effect of chloride ions and magnetite on the corrosion of Alloy 690 in alkaline solutions, Corrosion 73 (2017) 216-220.
[7] G.D. Song, W.I. Choi, S.H. Jeon, J.G, Kim, D.H. Hur, Combined effects of lead and magnetite on the stress corrosion cracking of Alloy 600 in simulated PWR secondary water, J. Nucl. Mater. 512 (2018) 8–14.
[8] G.D. Song, S.H. Jeon, Y.H. Son, J.G, Kim, D.H. Hur, Galvanic effect of magnetite on the corrosion behavior of carbon steel in deaerated alkaline solutions under flowing conditions, Corrosion Science 131 (2018) 71–80.
[9] W.I Choi, G.D. Song, S.H. Jeon, S.J. Kim, D.H. Hur, Magnetite-accelerated stress corrosion cracking of Alloy 600 in water containing 100 ppm lead oxide at 315 °C, J. Nucl. Mater. 522 (2019) 54–63.
[10] P.L. Andersen, Effects of temperature on crack growth rate in sensitized type 304 stainless steel and Alloy 600, Corrosion 49 (1993) 714–725.
[11] S.S. Hsu, S.C. Tsai, J.J. Kai, C.H Tsai, SCC behavior and anodic dissolution of Inconel 600 in low concentration thiosulfate, J. Nucl. Mater. 184 (1991) 97–106.